

## Role of projectile electrons in secondary electron emission from solid surfaces under fast-ion bombardment

A. Clouvas

*Department of Electrical and Computer Engineering, Aristotle University of Thessaloniki, GR-54006 Thessaloniki, Greece*

C. Potiriadis

*Greek Atomic Energy Commission, GR-15310 Agia Paraskevi, Greece*

H. Rothard

*Centre Interdisciplinaire de Recherches avec les Ions Lourds, Laboratoire Mixte CEA-CNRS, CIRIL-Boîte Postale 5133, F-14040 Caen, France*

D. Hofmann, R. Wünsch, and K. O. Groeneveld

*Institut für Kernphysik der J. W. Goethe Universität, August-Euler-Strasse 6, D-60486 Frankfurt am Main, Germany*

A. Katsanos

*Technical University of Krete, GR-73100 Chania, Greece*

A. C. Xenoulis

*Institute of Nuclear Physics, N.C.S.R. Demokritos, GR-15310 Agia Paraskevi, Greece*

(Received 9 December 1996; revised manuscript received 27 January 1997)

We report on measurements of the number of electrons per incoming projectile emitted from the projectile entrance and exit surfaces of thin carbon foils as function of the projectile atomic number  $Z$  ( $1 \leq Z \leq 32$ ), incident charge states, and velocities below, near, and above the stopping power maximum. The screening of the projectile charge by the projectile electrons reduces the backward electron emission. The corresponding reduction parameters have been determined as function of the number of projectile electrons. For all ions but protons we note as a general trend that the forward to backward yield ratio  $R_\gamma$  increases with the projectile velocity. In addition a pronounced increase of the  $R_\gamma$  with increasing  $Z$  is also observed. It was found that the increase of the  $R_\gamma$  with  $Z$  in the medium velocity region ( $\sim 1$  MeV/u) is not a ‘‘nuclear charge’’ effect, but is simply due to the difference in the incident number of projectile electrons. The experimental results are compared to Monte Carlo simulations based on the work by Gervais and Bouffard. A reasonable agreement (within 20%) between experimental and calculated results for heavy ions is observed. However, the difference is larger for light ions. Finally, the results are discussed within the framework of previously published semi-empirical models and the relation between electron yields and the electronic stopping power is elaborated. [S0163-1829(97)00118-5]

### I. INTRODUCTION

The interaction of fast charged particles with a condensed medium leads to particle emission from the solid surface, in particular to electron emission, the so-called ‘‘Kinetic electron emission,’’ which was described nearly 100 years ago.<sup>1</sup> The knowledge of the number of electrons emitted per incoming projectile (the electron yield  $\gamma$ ) as well as their angular and energy distribution is of fundamental interest. Important applications concern track formation in solids, heavy particle detectors, tumor treatment by heavy ion beams, effects of cosmic rays on crew and electronic devices in spacecraft, just to name a few. Recent extensive reviews on electron emission from solids can be found in Refs. 2–9. Most of these reviews refer to experimental and theoretical studies which have been performed on electron emission induced by

slow ( $< 25$  keV/u) or medium velocity ions ( $< 1$  MeV/u). Studies in the energy range  $E = 2 - 10$  MeV/u are sparse,<sup>10–13</sup> and studies in the high-energy region (10–100 MeV/u) (Refs. 14–17) and for relativistic projectiles ( $> 100$  MeV/u),<sup>18</sup> can still be considered as ‘‘pioneering work.’’

It is particularly astonishing that no systematic data exist of the projectile atomic number  $Z$  dependence of ion-induced electron emission from the entrance and exit surface of thin foils even in the medium projectile energy region. Therefore we measured the number of electrons per incoming projectile, i.e., the electron yield  $\gamma$ , from the beam entrance ( $\gamma_B$ ) and exit surfaces ( $\gamma_F$ ) of thin carbon foils ( $d = 1000$  Å) bombarded with 15 projectiles (ranging from  $Z = 1$  to  $Z = 32$ ) with different incident charge states  $q_i$  and different velocities,  $v$  below, near, and above the stopping power maximum. In the following, after a short description

of the experimental setup, we present the experimental results. They are discussed within the framework of widely used semiempirical models, and compared to Monte Carlo simulations. In particular the role of projectile electrons in secondary electron emission by fast-ion bombardment is elaborated.

## II. EXPERIMENT

The experimental work was performed at the 5-MV Tandem accelerator of the National Research Center of Physical Sciences ‘‘Demokritos’’ in Athens, Greece. Mass analyzed beams of

$$\begin{aligned}
 & \text{H}^+ \quad (1 \leq E \leq 7.5 \text{ MeV}); \\
 & \text{Li}^{q+} \quad (q=2-3)(1 \leq E \leq 14 \text{ MeV}); \quad \text{Be}^{q+} \quad (q=2-4)(8 \leq E \leq 18 \text{ MeV}); \\
 & \text{B}^{q+} \quad (q=2-4)(6 \leq E \leq 18 \text{ MeV}); \quad \text{C}^{q+} \quad (q=3-4)(6 \leq E \leq 16 \text{ MeV}); \\
 & \text{O}^{q+} \quad (q=3-5)(6 \leq E \leq 20 \text{ MeV}); \quad \text{F}^{q+} \quad (q=3-5)(8 \leq E \leq 24 \text{ MeV}); \\
 & \text{Al}^{q+} \quad (q=4-6)(15 \leq E \leq 27 \text{ MeV}); \quad \text{Si}^{q+} \quad (q=4-6)(9 \leq E \leq 27 \text{ MeV}); \\
 & \text{S}^{q+} \quad (q=4-6)(10 \leq E \leq 26 \text{ MeV}); \quad \text{Cl}^{q+} \quad (q=4-7)(10 \leq E \leq 30 \text{ MeV}); \\
 & \text{V}^{q+} \quad (q=5-7)(16 \leq E \leq 30 \text{ MeV}); \quad \text{Ni}^{q+} \quad (q=5-8)(11 \leq E \leq 34 \text{ MeV}); \\
 & \text{Cu}^{q+} \quad (q=6-8)(16 \leq E \leq 32 \text{ MeV}); \quad \text{Ge}^{q+} \quad (q=6-7)(18 \leq E \leq 27 \text{ MeV});
 \end{aligned}$$

were sent through thin  $16 \mu\text{g}/\text{cm}^2$  self-supporting carbon foils. The thicknesses of the targets were large enough to ensure that (a) the charge equilibrium of the penetrating particles was reached before the ions reach the exit surface and (b) full development of the secondary electron cascade induced by high-energy  $\delta$  electrons is reached. This is true for all incident ions except for fast proton beam.

The experimental setup used for these measurements is shown in Fig. 1. Two nearly closed metal cylinders (similar to Faraday cages, except for openings for the incoming and outgoing ion beam) mounted on each side of a target-foil holder were used to collect the secondary electrons in forward and backward directions of the target foil simultaneously but separately. The cylinders were held at a positive potential  $+U_0 = +40 \text{ V}$  to assure that all the secondary electrons were collected, and a negative potential of  $-U_0 = -20 \text{ V}$  was applied to the target, enough for the electron emission  $\gamma$  to reach a saturation value.<sup>19</sup> The Faraday cup was comprised of two parts: a beam-collecting cup that was grounded through the electrometer and a cylindrical electrode upstream of this cup (Repeller II) which was biased  $-U_{\text{rep}} = -300 \text{ V}$  with respect to the ground. This negatively biased electrode prevented (i) secondary electrons from escaping from the collecting cup and (ii) secondary electrons of the target from escaping through the opening of the outgoing ion beam of the second cylinder ( $\gamma$  cup). A similar repeller (Repeller I) was positioned upstream of the first  $\gamma$

cup and biased  $-U_{\text{rep}} = -300 \text{ V}$  with respect to the ground in order to prevent (i) secondary electrons from the slits to hit the first  $\gamma$  cup and (ii) secondary electrons of the target from escaping through the opening of the incoming ion beam of the first  $\gamma$  cup.

Backward ( $\gamma_B$ ), forward ( $\gamma_F$ ), and total ( $\gamma_T$ ) electron yields can easily be deduced from measuring: the ion-induced target current  $I_T$ , the current of low-energy electrons  $I_B$  and  $I_F$ , and the ion-beam current  $I_{FC}$ :

$$\gamma_B = q_f \left( \frac{I_B}{I_{FC}} \right), \quad (1)$$

$$\gamma_F = q_f \left( \frac{I_F}{I_{FC}} \right), \quad (2)$$

$$\gamma_T = q_f \left( \frac{I_T}{I_{FC}} \right) + q_f - q_i, \quad (3)$$

where  $q_f$  is the mean final charge state of the projectiles after leaving the foil exit surface, and  $q_i$  is the projectile incident charge before the foil entrance. The mean charge  $q_f$  of the projectiles emerging from the carbon foils was obtained from Shima *et al.*<sup>20</sup>

The secondary-electron coefficients  $\gamma_B$ ,  $\gamma_F$ , and  $\gamma_T$  have been measured as a function of the projectile atomic number  $Z$ , initial charge state  $q_i$ , and velocity  $v$  under standard vacuum conditions ( $P \approx 10^{-4} - 10^{-5} \text{ Pa}$ ). The error is estimated to be  $\pm 10\%$  (based on reproducibility measurements) for all the secondary electron yields. The thin self-supporting target foils have been produced by standard evaporation techniques at the Institut de Physique Nucléaire in Lyon, France. We assume a density of our carbon foils to be  $\rho = 1.65 \text{ g cm}^{-3}$ . This value has been obtained by an interferometric method and Rutherford-scattering analysis.<sup>21</sup>

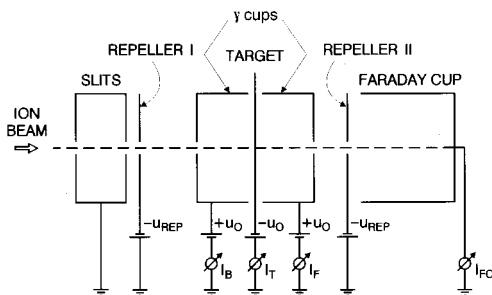


FIG. 1. Schematic experimental setup.

TABLE I. Backward ( $\gamma_B$ ), forward ( $\gamma_F$ ), total ( $\gamma_T$ ) electron yields for different incident ions with different incident charge states ( $q_i$ ) and energies ( $E$ ).

Ion	$q_i$	$E$ (MeV)	$\gamma_B$ $e^-/\text{ion}$	$\gamma_F$ $e^-/\text{ion}$	$\gamma_T$ $e^-/\text{ion}$	Ion	$q_i$	$E$ (MeV)	$\gamma_B$ $e^-/\text{ion}$	$\gamma_F$ $e^-/\text{ion}$	$\gamma_T$ $e^-/\text{ion}$
H	1+	1	1.07	1.48	2.55	C	4+	14	11.2	24.5	36
H	1+	1.5	0.86	1.19	2.05	C	4+	16	11	24	35
H	1+	2	0.69	0.97	1.68						
H	1+	2.5	0.64	0.83	1.48	O	3+	6	21.4	51.5	73.7
H	1+	3	0.54	0.72	1.27	O	3+	8	19.4	47.3	67.1
H	1+	3.5	0.48	0.63	1.13	O	3+	10	18.9	46.1	65.9
H	1+	4	0.43	0.55	0.98	O	3+	12	16.4	42.8	59.2
H	1+	4.5	0.4	0.52	0.93	O	3+	14	16	42.4	58
H	1+	5	0.39	0.5	0.9	O	4+	8	20	46.9	67.4
H	1+	5.5	0.36	0.45	0.81	O	4+	10	19.5	45.9	65.5
H	1+	6	0.33	0.42	0.75	O	4+	12	17.6	42.6	60.2
H	1+	6.5	0.32	0.39	0.72	O	4+	14	16.5	39.7	56.3
H	1+	7	0.3	0.37	0.67	O	4+	16	15.3	38.06	53.84
H	1+	7.5	0.29	0.35	0.64	O	5+	10	22.7	49.9	73.4
						O	5+	12	20.9	46.6	67.8
Li	2+	4	7.23	12.50	19.10	O	5+	14	18.6	42.55	62.15
Li	2+	6	6.53	11.09	16.60	O	5+	16	18	41.6	60.2
Li	2+	8	5.60	9.95	15.01	O	5+	18	16.4	38.4	54.3
Li	2+	10	5.00	9.02	13.70	O	5+	20	15.8	38.7	54.6
Li	3+	8	6.70	9.91	16.00						
Li	3+	10	5.98	9.09	14.90	F	3+	8	24.4	56.8	81.6
Li	3+	12	5.37	8.00	13.26	F	3+	10	22.4	50.3	81.5
Li	3+	14	5.00	7.48	12.60	F	3+	12	19.6	53	73
						F	3+	14	19.3	52.9	72.3
Be	2+	8	6.92	17.71	25.5	F	4+	10	21.1	53.2	74.9
Be	2+	10	6.25	16.43	22.65	F	4+	12	20	51	69.3
Be	3+	10	6.97	16.28	23.21	F	4+	14	19	49	67
Be	3+	12	6.47	15.25	21.65	F	4+	16	18	48.5	66
Be	3+	14	6.11	13.97	20.11	F	4+	18	17.8	47.55	65.1
Be	4+	16	6.9	12.78	20.7	F	4+	20	17.4	47	64.5
Be	4+	18	6.49	12.04	19.05	F	5+	10	24.4	56.8	81.6
						F	5+	12	23	54.5	77.8
B	2+	6	11.8	25.44	37.92	F	5+	14	21.2	51.7	71.5
B	2+	8	10.6	25.44	37.92	F	5+	16	20.3	50.6	69.4
B	3+	8	11.3	24.22	35.8	F	5+	18	19.4	48.6	66.9
B	3+	10	10.3	23.2	34.2	F	5+	20	18.7	47.5	65
B	3+	12	9.66	22.03	32.5	F	5+	22	18.5	46.93	63.39
B	3+	14	9.09	21.13	30.6	F	5+	24	17.5	45.2	63.67
B	4+	12	11.4	21.96	34.68						
B	4+	14	11	21.43	31.38	Al	4+	15	29	93.7	124
B	4+	16	10	19.85	30.43	Al	4+	17	27.2	87.5	116.5
B	4+	18	9.77	19.34	28.82	Al	4+	19	26.4	86.75	115.4
						Al	5+	15	31	90	121
C	3+	6	14.8	32.2	46.8	Al	5+	17	30	95	125
C	3+	8	13	28	41.6	Al	5+	19	29.5	94.68	121.8
C	3+	10	12	27	39	Al	5+	21	29.3	94.7	122.6
C	3+	12	11	24	35	Al	5+	23	28.4	92.3	121.9
C	3+	14	11	26	36	Al	6+	21	29.1	87.3	115.9
C	4+	8	14.4	29.2	44.2	Al	6+	23	28.2	86.4	112.5
C	4+	10	13.5	28	42	Al	6+	25	29.7	90.7	117.9
C	4+	12	12.5	27	39.6	Al	6+	27	29.8	91.7	119.8

TABLE II. Backward ( $\gamma_B$ ), forward ( $\gamma_F$ ), total ( $\gamma_T$ ) electron yields for different incident ions with different incident charge states ( $q_i$ ) and energies ( $E$ ).

Ion	$q_i$	$E$ (MeV)	$\gamma_B$ $e^-/\text{ion}$	$\gamma_F$ $e^-/\text{ion}$	$\gamma_T$ $e^-/\text{ion}$	Ion	$q_i$	$E$ (MeV)	$\gamma_B$ $e^-/\text{ion}$	$\gamma_F$ $e^-/\text{ion}$	$\gamma_T$ $e^-/\text{ion}$
Si	4+	9	30.5	87.4	119.5	Cl	6+	20	31.7	120.8	155.7
Si	4+	12	29	89.7	120	Cl	6+	22	32	123.5	153
Si	4+	15	28.4	93.8	124.8	Cl	6+	24	31.9	123.8	159
Si	4+	18	28.3	94.6	125.5	Cl	6+	26	31.3	124.3	156.7
Si	5+	12	32.1	93.6	127	Cl	7+	18	33.2	118.6	152
Si	5+	15	29.7	91.5	122.8	Cl	7+	20	33.2	120.9	156
Si	5+	18	28.6	89.8	121	Cl	7+	22	33.3	122.2	159
Si	5+	21	27.9	89.5	119.7	Cl	7+	24	33.3	124.4	160.6
Si	5+	24	27.2	89.7	118.2	Cl	7+	26	33.9	124.6	161.4
Si	6+	12	34	95.5	129.8	Cl	7+	28	33.3	124.5	159.5
Si	6+	15	35.7	98.2	135.7	Cl	7+	30	32.7	125.3	158
Si	6+	18	33	95.6	126						
Si	6+	21	31	89.8	117.5	V	5+	16	35.4	122.4	160.8
Si	6+	24	29.1	87.7	118.4	V	5+	18	36.2	132	171.3
Si	6+	27	28.7	88.1	117	V	5+	20	37.3	140.5	180.4
						V	5+	22	36.8	147	187.6
S	4+	10	28.4	98.6	128.7	V	6+	14	35.2	110.8	147.2
S	4+	12	28.1	106.4	136.6	V	6+	16	37	120.9	159.4
S	4+	14	28.3	111	142.7	V	6+	18	39.6	126.2	167.7
S	4+	16	28	113.6	143.8	V	6+	20	40	134	177
S	4+	18	28	114.5	145	V	6+	22	40.6	142.1	184.4
S	5+	12	29.7	106.4	137.9	V	6+	24	41	148.3	191.5
S	5+	14	29.7	110.6	142.2	V	6+	26	41.1	154	197.6
S	5+	16	29.3	111.8	141.7	V	7+	22	40.3	149.8	187.6
S	5+	18	29.7	116.6	145.9	V	7+	24	39.9	152.5	185.3
S	5+	20	28.8	114.6	145.4	V	7+	26	40.6	157.6	199.9
S	5+	22	28.6	115.8	145.5	V	7+	28	41	161	205.3
S	6+	14	30.8	111.4	145.5	V	7+	30	41.3	164.3	199.2
S	6+	16	30.2	113.7	148						
S	6+	18	30.5	115.4	149.5	Ni	5+	11	36.4	95.7	132.6
S	6+	20	29.8	115	148.4	Ni	5+	15	41	119	165.2
S	6+	22	29.8	114	145.4	Ni	6+	15	42.7	122.4	166
S	6+	24	30.1	115.7	146.8	Ni	6+	20	49	152	204
S	6+	26	29.6	115.6	146.4	Ni	7+	30	52.3	186.8	242.2
						Ni	8+	30	53	182	238
Cl	4+	10	28.7	95.94	125.3	Ni	8+	34	55	193.1	249.8
Cl	4+	12	29.3	103.7	133.6						
Cl	4+	14	29.7	112.6	143	Cu	6+	16	42.3	120.7	163.8
Cl	4+	16	30.5	119	149.5	Cu	6+	22	50	159	208
Cl	4+	18	30.3	121.3	149.7	Cu	6+	26	54.4	177	231
Cl	5+	12	30.9	108.7	139.2	Cu	7+	22	52.5	159.5	209
Cl	5+	14	30.9	114	147.1	Cu	7+	28	54	183	245
Cl	5+	16	30.7	117.4	148.1	Cu	8+	32	58	194	256
Cl	5+	18	30.4	119.3	146.6						
Cl	5+	20	30.6	122.7	152.3	Ge	6+	18	37	131	172
Cl	5+	22	30.5	123.5	154.5	Ge	6+	21	40	150	191
Cl	6+	14	31.9	113	147.4	Ge	6+	24	42.5	166	211
Cl	6+	16	32	116.7	146.6	Ge	7+	24	44.5	165	212
Cl	6+	18	32	119	149.7	Ge	7+	27	46.2	179	226

### III. RESULTS AND DISCUSSION

#### A. Presentation of the results

The  $\gamma_B$ ,  $\gamma_F$ ,  $\gamma_T$  yields for 15 projectiles with different incident energies ( $1 \leq E \leq 32$  MeV) and different incident charge states ( $1 \leq q_i \leq 8$ ) are shown in Tables I and II. The error for all coefficients is estimated to be  $\pm 10\%$ . The total electron yield  $\gamma_T$  has been measured previously in the same

laboratory. Within 10% we find the same values of  $\gamma_T$  as previously measured. As an example for incident protons, shown in Fig. 2 (triangles) are the  $\gamma_T$  values measured in the same laboratory in 1988 (Ref. 23).

For all ions we observe that within 2%

$$\gamma_T = \gamma_F + \gamma_B, \quad (4)$$

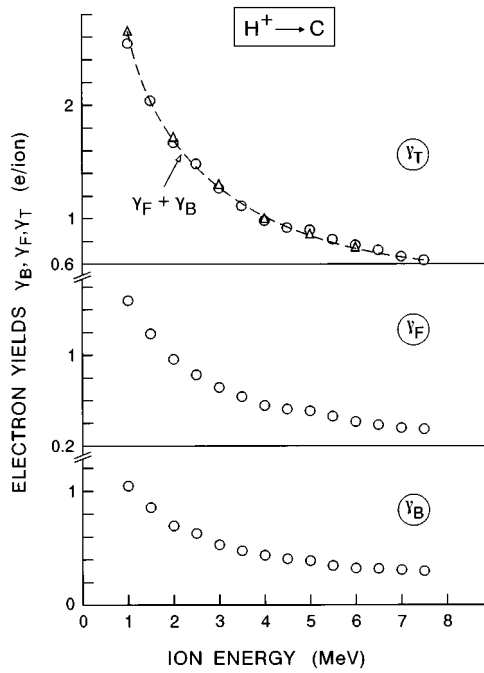


FIG. 2. Energy dependence of the backward, forward, and total secondary-electron yields for protons impinging on a thin carbon foil. Dashed line is the sum  $\gamma_F + \gamma_B$  and triangles are previous results obtained in the same laboratory (Ref. 23).

(e.g., see Fig. 2 dashed line). This observation does not only “test” the accuracy of the experimental setup but it means also that in the energy regime studied, the emission of high-energy  $\delta$  electrons is negligible in comparison to the low-energy electron emission. Indeed, electrons with energies ex-

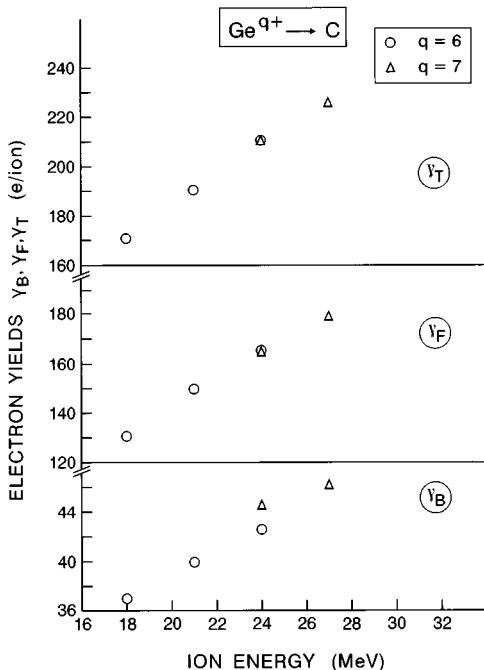


FIG. 3. Energy dependence of the backward, forward, and total secondary-electron yields for Ge ( $Z=32$ ) ions impinging on a thin carbon foil.

ceeding 300 eV, which are emitted in extreme forward or backward direction, can escape from the cups (e.g., see Refs. 14, 17, and Fig. 1). Thus the quantity  $\gamma_T - (\gamma_F + \gamma_B)$  gives qualitative information about high-energy  $\delta$  electrons. For the projectile energies used in this work the  $\delta$  electrons represent less than 2% of the total electron yield in quite good agreement with the 2–5 % observed with ions of similar velocities.<sup>12,22</sup> From 9.6 MeV/u up to 13.6 MeV/u,<sup>14</sup> they represent about 15–22 %. At 74 MeV/u, up to 35% of all electrons are “fast.”<sup>17</sup>

**B. Projectile atomic number and energy dependence of the secondary electron yields**

In the measured projectile velocity range, the energy dependence of the  $\gamma_B$ ,  $\gamma_F$ ,  $\gamma_T$  values for the different ions can be divided into three groups. For ions heavier than Cl ( $Z > 17$ )  $\gamma_B$ ,  $\gamma_F$ ,  $\gamma_T$  increase with the projectile energy (e.g., Fig. 3). For ions with  $Z$  between 13 and 17  $\gamma_B$ ,  $\gamma_F$ ,  $\gamma_T$  reach a maximum value (e.g., Fig. 4) and for ions  $1 \leq Z \leq 13$  the  $\gamma_B$ ,  $\gamma_F$ ,  $\gamma_T$  yields decrease with the projectile energy (e.g., Fig. 5). For a fixed projectile velocity the  $\gamma$  yields always increase with the projectile atomic number  $Z$  (Fig. 6). These facts can be understood from the proportionality between the electron emission yields and the stopping power  $dE/dx$ . In the energy regime studied the stopping power increases with the projectile energy for  $Z > 17$  ions, goes through its maximum for  $13 \leq Z \leq 17$  ions, and decreases with the projectile energy for  $Z < 13$  ions. In addition, for a given projectile velocity the stopping power indeed increases with the projectile atomic number  $Z$ .

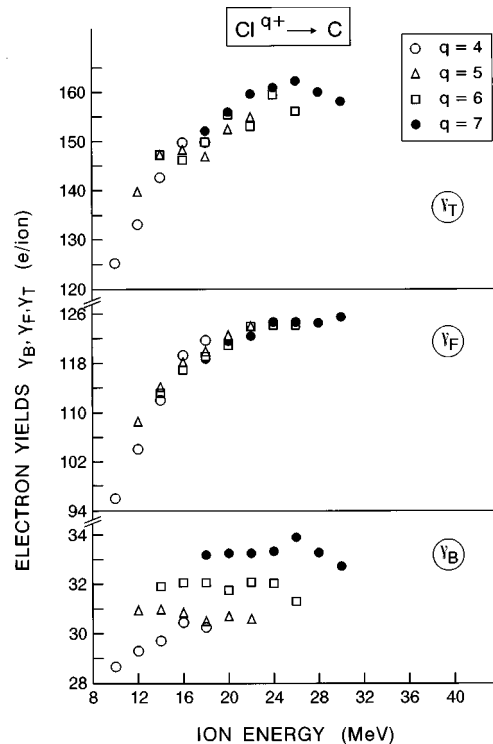


FIG. 4. Energy dependence of the backward, forward, and total secondary-electron yields for Cl ( $Z=17$ ) ions impinging on a thin carbon foil.

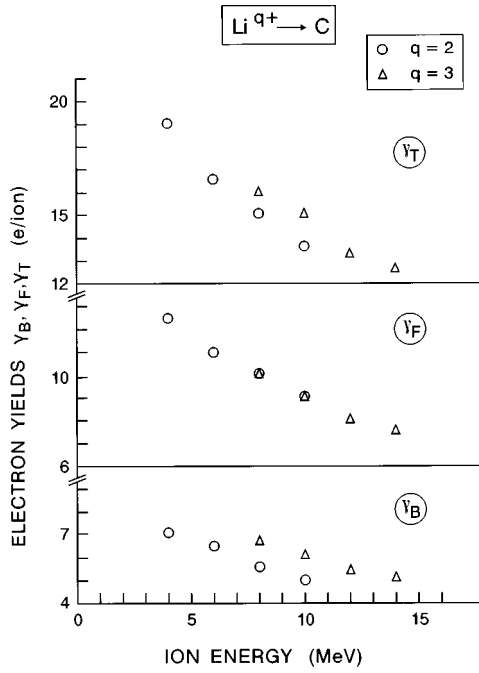


FIG. 5. Energy dependence of the backward, forward, and total secondary-electron yields for Li ( $Z=3$ ) ions impinging on a thin carbon foil.

### C. Incident charge-state dependence of the secondary electron yields

A dependence of the backward yield  $\gamma_B$  on the incident charge state  $q_i$  is observed for all projectiles. For a fixed projectile atomic number and velocity the  $\gamma_B$  increase with increasing  $q_i$  (e.g., Fig. 4). On the contrary, for almost all projectiles an independence of the forward yield  $\gamma_F$  from the incident charge state is observed (e.g., Figs. 3–5).

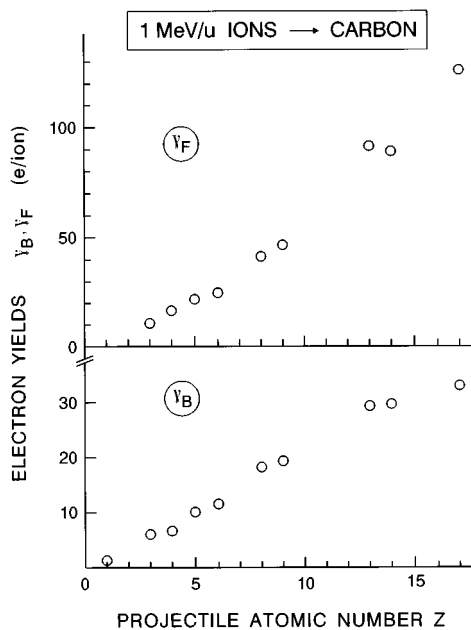


FIG. 6. Projectile atomic number,  $Z$ , dependence of the backward and forward yields for 1 MeV/u ions impinging on a thin carbon foil.

The above experimental observations can be understood within the framework of a semiempirical theory of electron emission introduced by Sternglass<sup>26</sup> and extended to thin foil targets including forward electron emission by Koschar *et al.*<sup>12</sup> and very recently by Rothard and co-workers.<sup>14,17</sup> One of the final results of this semiempirical theory are simple equations for  $\gamma_F$  and  $\gamma_B$  electron yields:

$$\gamma_B = \Lambda_C B_s (dE/dx)_{x=0}, \quad (5)$$

$$\gamma_F = \Lambda_C (dE/dx)_{x=d}, \quad (6)$$

where  $(dE/dx)_{x=0}$  and  $(dE/dx)_{x=d}$  denotes the projectile energy loss in the entrance and exit surface of the foil, respectively,  $\Lambda_C$  is a constant which mainly depends on the target material, and final  $B_s$  is the fraction of the projectile energy lost in soft collisions with large impact parameters, leading to direct production of low-energy electrons (or to plasmon excitation with subsequent electron production by plasmon decay). Following Eqs. (5) and (6) for a given projectile atomic number and velocity the backward yield  $\gamma_B$  must depend on the incident charge state  $q_i$ . According to Koschar *et al.*<sup>12</sup> and Rothard, Schou, and Groeneveld<sup>27</sup> the above dependence could be due to variations in stopping power near the entrance surface of the foil, which result from pre-equilibrium variations of the effective ion charge as a function of the penetration depth, since most of the emitted electrons originate from within a depth much smaller than the depth needed to reach charge equilibrium. For forward yields where the  $(dE/dx)_{x=d}$  at the exit surface of the foils is proportional to the effective charge of the ion near the exit surface, we must expect an independence of the forward yield  $\gamma_F$  from the incident charge state.

In order to quantify the charge-state dependence in the backward emission on incident  $q_i$  we define the ratio

$$V = \frac{\gamma_B^{q_i}}{\gamma_B^Z}, \quad (7)$$

which compares the electron yield  $\gamma_B^{q_i}$  of a projectile with  $(Z - q_i)$  electrons to the electron yield  $\gamma_B^Z$  of a projectile with zero electrons (bare projectile). The ratio  $V$  can give information about the role of the projectile electrons in the backward electron emission. Backward emission is due to the action of (a) the (partly screened, e.g., by  $K$ -shell electrons) positively charged nucleus and (b) the more loosely bound outer projectile electrons. As action (a) varies with the square of the (partly screened) nuclear charge, for heavy ions the contribution of projectile electrons in the backward emission is small compared to the contribution due to the nuclear charge. In this case  $V < 1$  and the ratio describes the screening effect of the nuclear charge by the projectile electrons concerning the production of secondary electrons.

In Fig. 7 is shown the ratio  $V$  for different hydrogenlike projectiles ( $Z - q_i = 1$ ) in the MeV/u energy range. The values for  $Z=3$  and  $Z=4$  are from the present work and the values for  $Z=1$ ,  $Z=2$ , and  $Z=6$  have been measured by some of us in Frankfurt.<sup>28–30</sup> In the same figure we present also the ratio  $\gamma_F^{q_i}/\gamma_F^Z$ . Indeed, the forward emission is independent of the incident charge state, thus the ratio of  $\gamma_F^{q_i}/\gamma_F^Z$  may be used as a test of the precision of the measure-

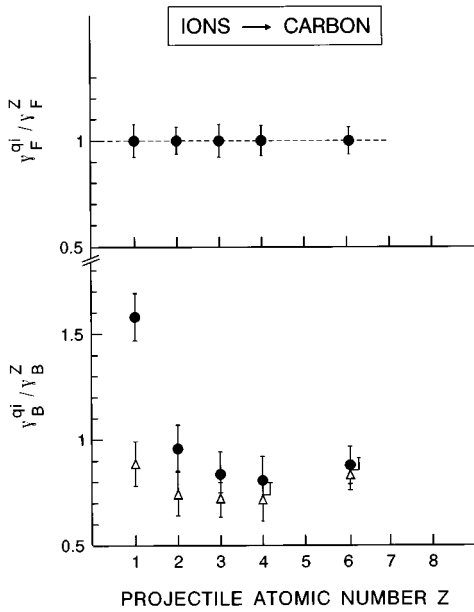


FIG. 7. Ratio  $\gamma_B^{q_i}/\gamma_B^Z$ , and  $\gamma_F^{q_i}/\gamma_F^Z$  for different hydrogenlike projectiles ( $Z - q_i = 1$ ) in the MeV/u energy range. The values for  $Z=1$ ,  $Z=2$ , and  $Z=6$  are from Refs. 28–30. In triangles are the  $\gamma_B^{q_i}/\gamma_B^Z$  values after subtraction of the projectile electron contribution to the  $\gamma_B$  yields.

ments. For all projectiles we observe, as we should, a ratio of  $\gamma_F^{q_i}/\gamma_F^Z$  equal to 1. For the backward emission the  $V$  ratio is about the same for projectiles with  $Z=2, 3, 4$ , and  $6$ . However, for hydrogen projectiles, the ratio  $V$  is larger than 1. This is caused by the contribution of the electron of the incident  $H^0$  beam to the  $\gamma_B$ . From recent measurements<sup>31</sup> performed in Caen of electron-induced electron emission from thin carbon foils, the contribution of the electron of incident hydrogenlike projectiles to  $\gamma_B^{q_i}$  can be estimated to be equal to 0.75 and can be subtracted from the measured  $\gamma_B^{q_i}$  yields. Here, we must assume that the projectile electrons contribute to the electron yield as a free electron of equal velocity. This should be a good approximation if the electrons are not strongly bound, i.e., for light ions (and in particular, fast  $H^0$  projectiles), electrons in excited projectile states, or even outer shell electrons of heavy ions. In Fig. 7 is presented (triangles) the  $V$  ratio after subtraction of the electron contribution to the  $\gamma_B^{q_i}$  yields. Again, an independence of  $V$  on  $Z$ , is observed within the experimental error.

The dependence of the  $V$  ratio on the number of the projectile electrons ( $Z - q_i$ ) for a number of 1 MeV/u incident projectiles is shown in Fig. 8. The value of  $\gamma_B^Z$  for ( $Z=6$ ) was obtained from Ref. 30. For incident oxygen and fluorine ions we did not have any available bare ions so the  $V$  ratio could not be directly deduced. To overcome the lack of data we assume that for ions with a small difference in  $Z$  the  $V$  ratio depends only on the number of projectile electrons and not on  $Z$ . This assumption is verified in Fig. 8 for hydrogenic and heliumlike projectiles. Based on this assumption the  $V$  ratio for oxygen and fluorine ions could be indirectly deduced. For oxygen ions with  $q_i=5$  (three projectile electrons) we assumed that the  $V$  ratio is equal to 0.63, obtained with C ions ( $q_i=3$ ) with the same number of projectile elec-

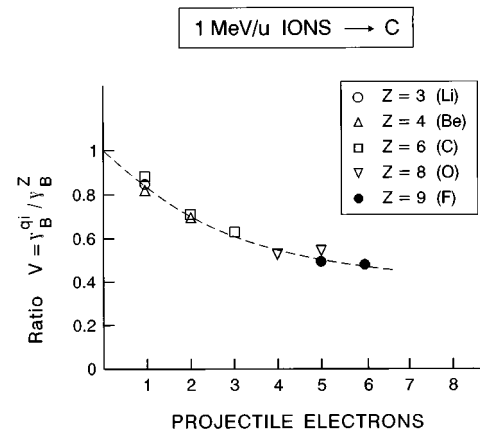


FIG. 8. Ratio  $V = \gamma_B^{q_i}/\gamma_B^Z$  as function of the number of projectile electrons of 1 MeV/u incident ions.

trons. Then, from the experimental ratios  $\gamma_B^{q_i=3,4}/\gamma_B^{q_i=5}$  the  $V$  ratio for oxygen ions with  $q_i=3$  and  $q_i=4$  has been obtained. In a similar way the  $V$  ratio for fluorine ions with  $q_i=3$  and  $q_i=4$  has been deduced.

The independence of the  $V$  ratio of  $Z$ , for a fixed number of projectile electrons, and the reduction of  $V$  as function of the number of projectile electrons clearly indicate that the critical parameter of the screening effect of the nuclear charge by the projectile electrons is the number of projectile electrons and not the nuclear charge.

#### D. Forward to backward yield ratio

Only with thin foils is it possible to study the forward to backward yield ratio  $R_\gamma = \gamma_F/\gamma_B$  introduced by Meckbach, Braunstein, and Arista in 1975.<sup>32</sup> This ratio contains information about the fraction of slow electrons produced by high-energy  $\delta$  electrons. Slow electrons are emitted isotopically, whereas fast electrons are peaked into the forward direction.  $R_\gamma$  increases with the proton energy (below 150 keV) and reaches a maximum value of about 1.5. When the proton energy is further enhanced up to 1 MeV, the ratio decreases slightly.<sup>33,34</sup> In Fig. 9 the ratio  $R_\gamma$  is presented for incident protons with energies 20 keV up to 7.5 MeV. The

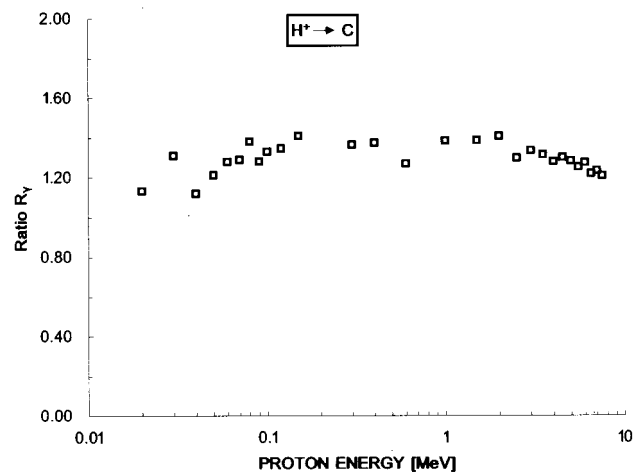


FIG. 9. Ratio  $R_\gamma = \gamma_F/\gamma_B$  as function of the proton energy. The values of  $R_\gamma$  for 20-keV protons up to 600 keV are from Ref. 33.

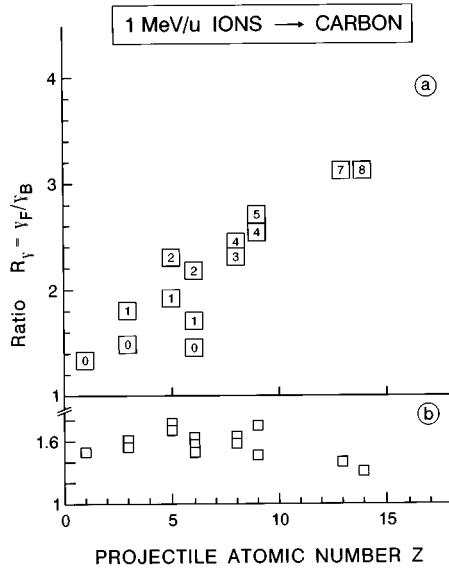


FIG. 10. (a)  $R_\gamma$  dependence as function of the projectile atomic number  $Z$  for 1 MeV/u projectiles with different incident charge states. The number inside the boxes indicate the number of projectile electrons. (b) The  $R_\gamma$  values of (a) are extrapolated to the values we would have obtained with fully stripped incident ions [see Eq. (8) and text].

values of  $R_\gamma$  for 20 keV up to 600 keV were obtained from Ref. 33. The experimental error of each measurement is about 10–20%. In general, a weak dependence of  $R_\gamma$  on the proton energy is observed. The values are clustered around a mean value of about 1.3, which means [Eqs. (5) and (6)] that about 77% of the proton energy is lost in soft collisions with large impact parameters leading to direct production of low-energy electrons (or to plasmon excitation with subsequent electron production by plasma decay).

A pronounced increase of  $R_\gamma$  as function of the projectile atomic number  $Z$  for 1 MeV/u projectiles with different incident charge states is shown in Fig. 10(a). The number inside the boxes indicate the number of projectile electrons. The error of each measurement is about 20%. Despite the fact that  $R_\gamma$  increases with  $Z$  it can be seen in Fig. 10(a) that for a given number of projectile electrons  $R_\gamma$  seems independent of  $Z$ . This is impressively shown in Fig. 10(b) where the  $R_\gamma$  values are “extrapolated” to the values  $R_\gamma^Z$  we would have obtained with fully stripped incident ions. The extrapolated  $R_\gamma^Z$  values were obtained from the following equation:

$$R_\gamma^Z = \frac{\gamma_F^Z}{\gamma_B^Z} = \left( \frac{\gamma_F^Z}{\gamma_F^{q_i}} \right) \left( \frac{\gamma_F^{q_i}}{\gamma_B^{q_i}} \right) \left( \frac{\gamma_B^{q_i}}{\gamma_B^Z} \right), \quad (8)$$

with  $0 \leq q_i \leq Z$ .

The term  $\gamma_F^Z / \gamma_F^{q_i}$  is equal to 1 (see Fig. 7). Indeed, for a given projectile the forward yield is independent of the incident charge state (e.g., Fig. 7). The term  $\gamma_F^{q_i} / \gamma_B^{q_i}$  is the measured  $R_\gamma$  value and the term  $\gamma_B^{q_i} / \gamma_B^Z$  corresponds to the ratio  $V$  for  $(Z - q_i)$  electrons which is given in Fig. 8. From Fig. 10 it is therefore clear that the increase of  $R_\gamma$  with  $Z$  in the medium velocity region ( $\sim 1$  MeV/u) is not a “nuclear

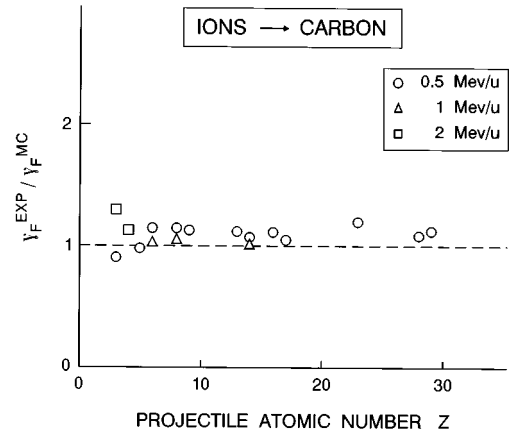


FIG. 11. Comparison between experimental results of the forward electron yields and Monte Carlo simulations for different projectile atomic number and velocities.

charge” effect but is simply due to the difference in the incident number of projectile electrons.

#### E. Comparison between the experimental results and Monte Carlo simulations

It is useful to use experimental results of electron emission as benchmark for the improvement of numerical simulation of the primary stage of ion-matter interaction. A sophisticated numerical simulation of energy deposition by heavy ions in solids was developed at CIRIL by Gervais and Bouffard.<sup>35</sup> It can also be used to calculate forward and backward electron yields.<sup>14</sup> The projectiles are treated as point charges of constant kinetic energy with an effective charge  $q^*(z, v)$ . The target material carbon is characterized by its atomic number and mass ( $Z=6$ ,  $A=12$ ), density ( $\rho = 1.65 \text{ g cm}^{-3}$ ), Fermi energy  $E_F = 17 \text{ eV}$ , and corresponding plasmon excitation frequency ( $h\omega = 2.12 \text{ eV}$ ), and the  $1_s$  ionization energy  $U_{1s} = 284 \text{ eV}$ . For the calculation of electron yields, all electrons liberated by a primary ionization (projectile) event at a point  $x'$  inside the target,  $0 \leq x' \leq d$ , or by secondary ionization (primary electron) events are followed from their point of liberation until they reach either the backward surface or the forward surface. If their kinetic energy (with respect to the Fermi energy) is higher than the workfunction of  $\Phi \cong 5 \text{ eV}$ , they are considered as being ejected into the vacuum and counted for the calculation of the forward and backward electron yields. The model is described in detail in Refs. 14, 17, and 35. At this stage, the simulation cannot give realistic calculations of backward yields as the evolution of the incident projectile charge state with penetration depth is not considered. In the velocity region investigated here, the ionic charge state evolves even in the first layers of the solid and thus already over a penetration depth comparable to the slow electron escape depth. In contrast, the targets are thick enough to assure charge equilibration at the exit surface, so that here a constant projectile charge (approximated by the effective charge  $q^*$ ) is a good approximation. For this reason in Fig. 11 only the forward electron yields are compared with the calculated ones. A rather good agreement between experimental results and calculated values is observed (difference within 20%).

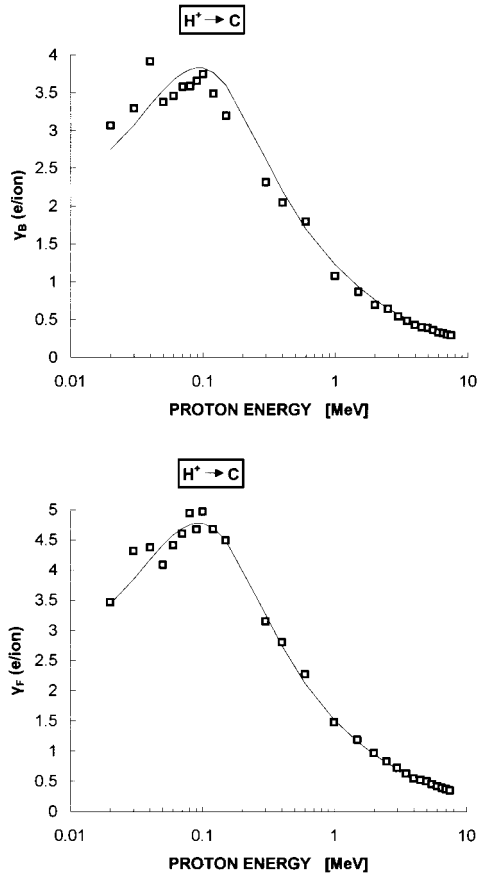


FIG. 12. Forward and backward electron yields ( $e/ion$ ) from thin carbon foils as function of the proton energy. The values of  $\gamma_F$  and  $\gamma_B$  for 20-keV protons up to 0.6 MeV are from Ref. 33. Equations (11) and (12) are represented by a solid line.

#### F. Proportionality between electron emission and stopping power

The proportionality between electron emission and stopping power predicted by the most important theoretical models<sup>2,12,26,27,36–38</sup> has been studied extensively during the last decade (e.g., Refs. 3, 9). In all studies it became common practice to define parameters  $\Lambda_{B,F,T}$  as ratios between the measured electron yields  $\gamma$  and the stopping power  $S$  values to study the validity of the proportionality as a function of the projectile velocity and atomic number and the target atomic number. We thus introduce the parameters:

$$\Lambda_T = \gamma_T / S, \quad (9)$$

$$\Lambda_B = \gamma_B / S, \quad (10)$$

$$\Lambda_F = \gamma_F / S. \quad (11)$$

For proton-induced electron emission from thin carbon foils the proportionality has been confirmed experimentally in a wide energy range, i.e.,  $20 \text{ keV} \leq E \leq 10 \text{ MeV}$  for  $\gamma_T$  (Refs. 34, 23, 33) and  $20 \text{ keV} \leq E \leq 1 \text{ MeV}$  for  $\gamma_F, \gamma_B, \gamma_T$  (Refs. 33, 34). In the present study, the measurement of the  $\gamma_F$  and  $\gamma_B$  yields was extended up to proton energy 7.5 MeV. In Fig. 12 the forward and backward electron yields from thin carbon foils are presented as a function of the proton energy. The values of  $\gamma_F$  and  $\gamma_B$  for 20-keV protons up to 0.6 MeV

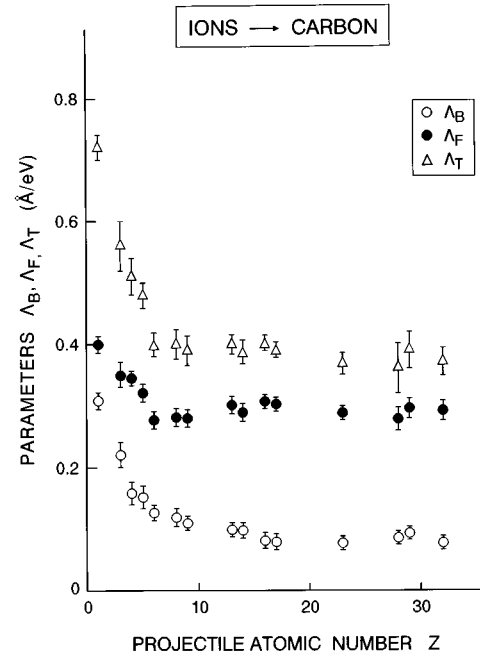


FIG. 13. Parameters  $\Lambda_B, \Lambda_F, \Lambda_T$  as function of the projectile atomic number. The values of  $\Lambda_{B,F,T}$  are the mean values of each projectile obtained with various incident projectile energies and initial charge states.

are from Ref. 33. The correlation analysis between the coefficients  $\gamma_F, \gamma_B$  and the stopping power  $S$  (in  $\text{eV}/\text{\AA}$ ) obtained from the TRIM code<sup>39</sup> give

$$\gamma_F = (0.40 \pm 0.006)S, \quad (12)$$

$$\gamma_B = (0.31 \pm 0.008)S \quad (13)$$

with  $r$  squared (validity of the correlation) equal to 98.3% for the backward emission and 99.4% for the forward emission. In Fig. 12, Eqs. (12) and (13) are represented by a solid line.

The  $\Lambda_F$  and  $\Lambda_B$  parameters as a function of the incident ion energy within an uncertainty of  $\pm 10\%$  are independent of the projectile velocity, a result which has been reported previously<sup>24,25</sup> for the  $\Lambda_T$  parameter. However for ions heavier than vanadium a slight increase of the  $\Lambda_F$  with the ion velocity is observed. In addition for incident protons is observed a small increase of the  $\Lambda_B$  parameter with the proton velocity. Recently Benka, Steinbauer, and Bauer<sup>40</sup> measured  $\gamma_B$  and  $S$  simultaneously for  $\text{H}^+$  and  $\text{He}^{++}$  impact (in the MeV energy range) on thick Ag, Al, and Cu targets. Due to the simultaneous measurement of  $\gamma_B$  and  $S$  they obtained very precise values of  $\Lambda_B$  (with an accuracy better than 2%). For proton impact on Ag and Cu targets, their  $\Lambda_B$  values are almost independent of  $\text{H}^+$  energy. For Al targets an increase of  $\Lambda_B$  with  $\text{H}^+$  energy was observed as in this work.

The  $\Lambda_B, \Lambda_F, \Lambda_T$  parameters are presented in Fig. 13 as function of the projectile atomic number. The values of  $\Lambda_{B,F,T}$  presented are the mean values of each projectile obtained with various incident projectile energies and initial charge states. The error bars include statistical fluctuations as well as the incident charge state and energy dependence of the electron yields.  $\Lambda_F$  and  $\Lambda_B$  parameters first decrease with

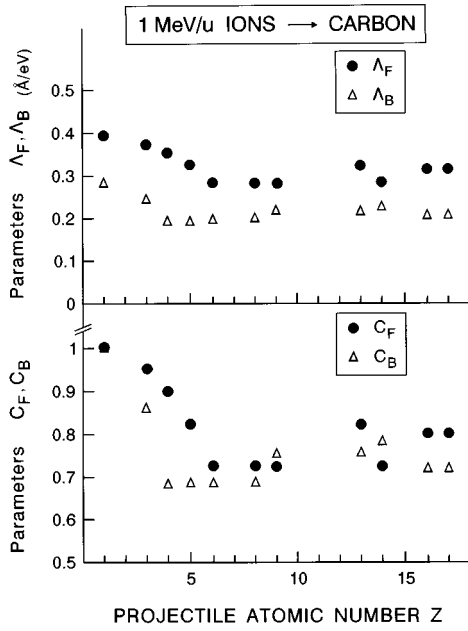


FIG. 14. Indirectly deduced  $Z$  dependence of  $\Lambda_B$  and  $\Lambda_F$  for 1 MeV/u bare ions (see text). In the lower part is presented the  $Z$  dependence of the ratios  $C_B$  and  $C_F$  defined by Eqs. (15) and (16).

$Z$  and reach a saturation value for the forward yield at  $Z > 6$  and for the backward yield at  $Z > 14$ .

The reduction of  $\Lambda(Z)$  values with increasing  $Z$  is stronger for the backward emission (60–70 %) than for forward emission (30–35 %). This could be partly due to the dependence of  $\gamma_B$  on the incident number of projectile electrons (incident charge state—screening). For light ions  $Z < 5$  we had used even bare ions, on the contrary, for the heavy ions  $Z > 13$  the number of projectile electrons was more than 7. It is therefore interesting to compare the  $Z$  dependence of  $\Lambda_B(Z)$  and  $\Lambda_F(Z)$  for incident isotachic bare ions. In Fig. 14 is presented the indirectly deduced dependence of  $\Lambda_B$  and  $\Lambda_F$  as function of the projectile atomic number for different incident 1 MeV/u bare ions. The  $\gamma_B^Z$  values corresponding to bare ions and consequently the  $\Lambda_B$  values [Eq. (10)] were deduced from the equation

$$\gamma_B^Z = \frac{\gamma_B^{q_i}}{V}, \quad (14)$$

where  $\gamma_B^Z$  is the deduced backward yield,  $\gamma_B^{q_i}$  is the measured backward yield, and  $V$  is the ratio obtained from Fig. 8 for  $(Z - q_i)$  projectile electrons. For the forward yield the  $\gamma_F$  values and consequently the  $\Lambda_F$  values are independent of the incident charge state and therefore the measured values of  $\Lambda_F$  obtained with different incident charge states can be used also for the bare ions. We observe in Fig. 14 that  $\Lambda_B$  and  $\Lambda_F$  have almost the same dependence as a function of the projectile atomic number. This can be clearly seen in the lower part of Fig. 14 where the ratios  $C_B$  and  $C_F$  defined in Eqs. (15) and (16) are presented as functions of the projectile atomic number  $Z$ :

$$C_B = \frac{\Lambda_B(Z)}{\Lambda_B(Z=1)}, \quad (15)$$

$$C_F = \frac{\Lambda_F(Z)}{\Lambda_F(Z=1)}. \quad (16)$$

The reduction of  $\Lambda(Z)$  values with increasing  $Z$  seems to be the same for backward and forward emission. The decrease of  $\Lambda_B$  and  $\Lambda_F$  with  $Z$  can be qualitatively understood from the preequilibrium stopping power concept introduced by Koschar *et al.*<sup>12</sup> The stopping powers used for calculation of the  $\Lambda_{B,F,T}$  parameters in expressions (9)–(11) are the computed bulk energy-loss values.<sup>39</sup> It is now well established [see Eqs. (5) and (6)] that “nonequilibrium near-surface stopping powers” both at the upstream and downstream surfaces of the foils are responsible for the production of the secondary electrons in the entrance and exit surface of the foil. The decrease of the  $\Lambda_B$  with  $Z$  for ions of about 0.1–1 MeV/u could be due to a reduced stopping power near the surface, which results from pre-equilibrium variation of the effective ion charge as a function of the penetration depth. In a similar way a reduction of the  $\Lambda_F$  parameter for the heavy ions can be expected due to variation of the effective ion charge upon exit from the downstream surface of the foil. The dependence of the effective ion charge  $q(x)$  inside a thin solid foil of thickness  $d$  as a function of the penetration depth was experimentally deduced for nitrogen and oxygen projectiles by Zaikov *et al.*<sup>41</sup> They found a smaller effective charge  $q^*(x=d)$  near the exit surface compared to the “bulk” effective charge. The data of Zaikov *et al.* do indeed suggest that charge exchange processes upon exit of the ions from the foils cannot be neglected. Also, the dynamic screening of the projectile charge and the population of excited states change upon exit. This could lead to (however, small) modifications of the effective charge which could still be felt in the last layers of the solid, since the ions begins to “see” the “boundary” surface before leaving the solid. For fast incident protons ( $E > 100$  keV) there is indeed no difference between the near-surface effective charge and the “bulk” effective charge and consequently between the near-surface stopping power and the tabulated bulk energy loss. Another possible mechanism to understand the reduction of the  $\Lambda_B$  and  $\Lambda_F$  parameters for the heavy ions is the energy deposition by nonionizing excitation of target atoms. According to Rothard, Schou, and Groeneveld<sup>27</sup> the dissipation of projectile energy in nonionizing events such as target or projectile excitation with subsequent photon emission is projectile dependent. The fraction  $r$  of the ion energy loss that does not contribute to the production of secondary electrons may be higher for heavy than for light ions.

In the above discussion we considered only mechanisms which are related to the production of secondary electrons. However, electron emission is not exclusively related to the production of secondary electrons. The kinetic emission of electrons is generally considered as a three-step process: (1) production of the secondary electrons; (2) transport of secondary electrons towards the entrance and exit surface of the foil; (3) escape of the secondary electrons from the target surfaces.

Mechanisms related to steps (2) and (3) may become important in particular for fast heavy ions due to the strong charge and induced ionization density. In Fig. 15 is presented the ratio  $\gamma_F/Z^2$  and  $\gamma_B/Z^2$  as function of the projectile atomic number for 2 MeV/u  $H^+$ ,  $Li^{3+}$ , and  $Be^{4+}$  ions. For

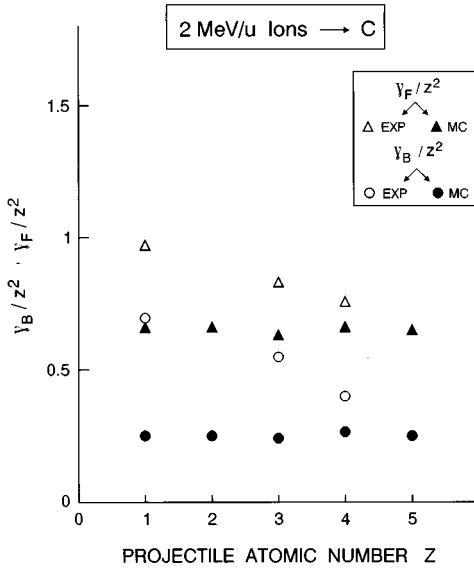


FIG. 15. Ratio  $\gamma_F/Z^2$  and  $\gamma_B/Z^2$  as function of the projectile atomic number for 2 MeV/u  $H^+$ ,  $Li^{3+}$ , and  $Be^{4+}$  ions. In close symbols are presented the calculated values for  $H^+$ ,  $He^+$ ,  $Li^{3+}$ ,  $Be^{4+}$ , and  $B^{5+}$  ions, by Monte Carlo simulations.

such fast bare ions the near surface stopping power is the same as the tabulated bulk stopping power  $S$  which is given by

$$S_z = Z^2 S_H. \quad (17)$$

The  $Z$  dependence of the ratios  $\gamma_F/Z^2$  and  $\gamma_B/Z^2$  have, in this case, the same meaning as the  $Z$  dependence of the  $\Lambda_F$  and  $\Lambda_B$  parameters, respectively. We observe a decrease of  $\gamma_B/Z^2$  and  $\gamma_F/Z^2$  with  $Z$  in contradiction with the Monte Carlo simulations based on the work of Gervais and Bouffard<sup>35</sup> where an independence of  $Z$  is calculated. The decrease of the  $\Lambda_B$  parameter as a function of  $Z$  for fast bare ions impinging on thick metal targets has been reported by Borovsky and Suszcynsky.<sup>13</sup> Similar results have been reported by Benka *et al.*<sup>42</sup> In order to interpret the decrease of the  $\Lambda_B$  parameter as a function of  $Z$  for fast bare ions Borovsky and Suszcynsky<sup>13</sup> proposed a model taking into account the electron trapping in the wake of the ion due to an attractive track potential. Consider a completely stripped ion of high enough velocity to ensure charge-state conservation over a penetration distance much larger than the electron escape depth. Such an ion produces, due to the high density of ionization, a positively charged track in its wake. As a result, the attractive track potential causes an attractive force which retains a certain number of the electrons liberated and moving away from the ion track. Consequently, electron yields will be reduced, with a yield reduction increasing with increasing  $Z$ . However, the model proposed by Borovsky and Suszcynsky<sup>13</sup> should not be invoiced uncritically. Following the arguments of Schiwietz and Xiao<sup>10</sup> collective effects in a metal will give rise to a wake potential which can be estimated from the linear-response free-electron-gas theory.<sup>43</sup> The first oscillation of the wake has the largest amplitude and it represents a repulsive potential for electrons and not an attractive one. Furthermore, wake calculations within second-order perturbation theory show no trend to-

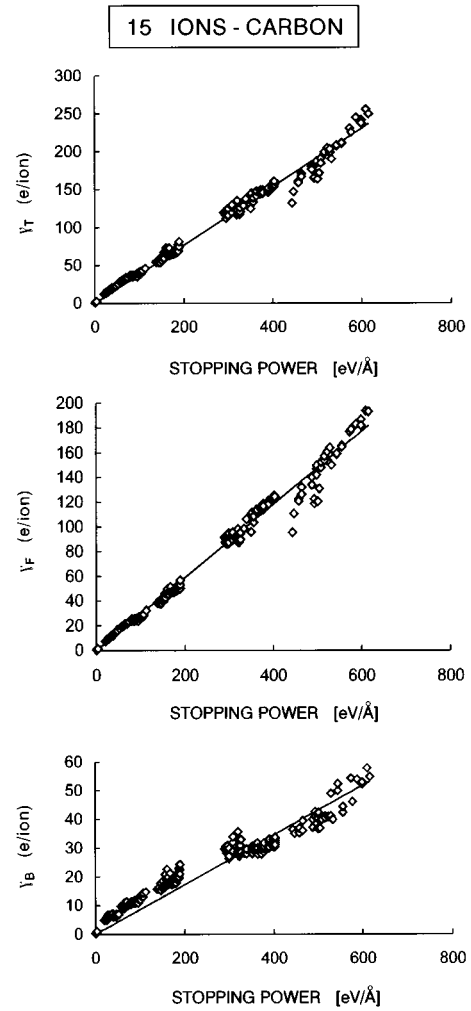


FIG. 16. Backward, forward, and total electron yields from carbon foils as a function of the stopping power  $S$  for 15 different projectiles with different projectile velocities and initial charge states. The straight lines represent Eqs. (18)–(20).

ward a reduced mobility of electrons for highly charged projectiles.<sup>44</sup> Thus, the proposed deceleration of electrons, due to a positively charged track<sup>13</sup> is inconsistent with the free-electron-gas theory of metals.

Despite the different mechanisms (pre-equilibrium near-surface stopping power, projectile or target excitation, and electric field in the ion wake) mentioned above to describe the  $Z$  dependence on the  $\Lambda_B$  and  $\Lambda_F$  parameters, the important assumption of an overall proportionality between the backward, forward, and total secondary-electron yields and the electronic loss (per unit path length) of the projectiles is demonstrated impressively in Fig. 16. The figure shows the backward, forward, and total secondary-electron yields from carbon foils as a function of the stopping power  $S$  for 15 different projectiles with different projectile velocities and initial charge states. The correlation analysis between the coefficients  $\gamma_B$ ,  $\gamma_F$ , and  $\gamma_T$  and the stopping power  $S$  (in eV/Å) for about 200 experimental values give

$$\gamma_B = (0.086 \pm 0.0008)S, \quad (18)$$

$$\gamma_F = (0.295 \pm 0.001)S, \quad (19)$$

$$\gamma_T = (0.385 \pm 0.002)S, \quad (20)$$

with  $r$  squared (validity of the correlation) equal to 93% for the backward yield, 98% for the forward yield, and 99% for the total yield. In Fig. 16, Eqs. (18)–(20) are represented by a straight line. In the correlation analysis we neglected any uncertainty in the stopping power  $S$  values which were simply obtained from Ref. 39.

#### IV. CONCLUSIONS

In this study we measured the number of electrons per incoming projectile from the beam entrance and exit surfaces of thin carbon foils bombarded with 15 projectiles ( $1 \leq Z \leq 32$ ) with different incident charge states and different velocities, below, near, and above the stopping power maximum. For the projectile energies used in this work, high-energy  $\delta$  electrons represent less than 2% of the total electron yield. A dependence of the backward yield  $\gamma_B$  on the incident charge state is observed for all projectiles while for most projectiles an independence of the forward yield  $\gamma_F$  from the incident charge state is observed. The screening of the projectile charge by the projectile electrons reduces the backward electron emission. The corresponding reduction parameters have been determined as a function of the number of the projectile electrons.

For all ions, except protons, we note as general trend that the forward to backward yield ratio  $R_\gamma$  increases with the projectile velocity. In addition, a pronounced increase of the  $R_\gamma$  with increasing  $Z$  is also observed. It was found that the increase of the  $R_\gamma$  with  $Z$  in the medium velocity region ( $\sim 1$  MeV/u) is not a “nuclear charge” effect, but is simply due to the difference in the incident number of projectile electrons.

We used the experimental results of electron emission as benchmark for improving the numerical simulation of the primary stage of ion-matter interaction. We performed Monte Carlo simulations based on the work by Gervais and Bouffard.<sup>35</sup> A reasonable agreement (within 20%) between experimental and calculated results for heavy ions is observed. However the difference is larger for light ions. In addition, the numerical simulation does not predict the de-

crease of  $\gamma_B/Z^2$  and  $\gamma_F/Z^2$  with  $Z$  for fast bare ions.

For nearly all projectiles in the velocity region studied here coefficients  $\gamma_F$  and  $\gamma_B$  and the stopping power  $S$  have the same velocity dependence. However for ions heavier than vanadium a slight increase of the parameter  $\Lambda_F = \gamma_F/S$  with the projectile energy may be stated. The systematic study of the  $\Lambda_B$  and  $\Lambda_F$  parameters as function of the projectile atomic number  $Z$  indicate a decrease with  $Z$  down to a saturation value after  $Z > 6$  for the forward yield and after  $Z > 14$  for the backward yield. The reduction effect is stronger for the backward emission than for forward emission, a fact which is due to the dependence of  $\gamma_B$  on the incident charge state. Possible reasons for the  $Z$  dependence of the  $\Lambda_B$  and  $\Lambda_F$  parameters are:

(i) The reduced pre-equilibrium near-surface stopping power (in comparison to the calculated by TRIM bulk energy-loss values) responsible for the production of secondary electrons in the entrance and exit surfaces of the foil; (ii) the fraction of the ion energy loss which leads to target (or projectile) excitation and consequently does not contribute to the production of secondary electrons; (iii) The electric field in the wake of a fast ion which inhibits the escape of Coulomb-scattered electrons, thereby reducing the secondary-electron yields. However, even if this mechanism can explain the experimental results obtained with fast bare ions, it is inconsistent with the free-electron-gas theory of metals.

Despite the different mechanisms mentioned above to describe the  $Z$  dependence of the  $\Lambda_{B,F,T}$  parameters, the important assumption of an overall proportionality between the backward, forward, and total secondary-electron yields and the stopping power is demonstrated impressively in Fig. 16.

#### ACKNOWLEDGMENTS

This work has been supported by and performed under the auspices of the German-Greek Research and Development Collaboration. H.R., D.H., R.W., K.O.G. wish to thank our Greek colleagues for the fruitful collaboration in Athens. H.R. thanks B. Gervais (CIRIL/CAEN) for important discussions and making accessible his numerical simulation. H.R. acknowledges travel support from the “Service Culturel et Scientifique” of the French embassy in Greece.

<sup>1</sup>M. P. Villard, J. Phys. Theor. Appl. **8**, 5 (1899).

<sup>2</sup>J. Devooght, J. C. Dehaes, A. Dubus, M. Cailler, J. P. Ganachaud, M. Rösler, and W. Brauer, in *Particle Induced Electron Emission I*, edited by G. Höhler and E. A. Niekisch, Springer Tracts in Modern Physics Vol. 122 (Springer, Berlin, 1991).

<sup>3</sup>D. Hasselkamp, H. Rothard, K. O. Groeneveld, J. Kemmler, P. Varga, and H. Winter, in *Particle Induced Electron Emission II*, edited by G. Höhler and E. A. Niekisch, Springer Tracts in Modern Physics Vol. 123 (Springer, Berlin, 1991).

<sup>4</sup>*Ionization of Solids By Heavy Particles*, Vol. 306 of *NATO Advanced Study Institute, Series B: Physics*, edited by R. Baragiola (Plenum, New York, 1993).

<sup>5</sup>R. A. Baragiola, Nucl. Instrum. Methods Phys. Res. Sect. B **78**, 223 (1993).

<sup>6</sup>J. Schou, Scanning Microsc. **2**, 607 (1988).

<sup>7</sup>W. O. Hofer, Scanning Microsc. Suppl. **4**, 265 (1990).

<sup>8</sup>B. A. Brusilovsky, Appl. Phys. A **50**, 111 (1990).

<sup>9</sup>H. Rothard, Scanning Microsc. **9**, 1 (1995).

<sup>10</sup>G. Schiwietz and G. Xiao, Nucl. Instrum. Methods Phys. Res. Sect. B **107**, 113 (1996).

<sup>11</sup>A. Koyama, T. Shikata, H. Sakairi, and E. Yagi, Jpn. J. Appl. Phys. **21**, 1216 (1982).

<sup>12</sup>P. Koschar, K. Kroneberger, A. Clouvas, M. Burkhard, W. Meckbach, O. Heil, J. Kemmler, H. Rothard, and K. O. Groeneveld, R. Schramm, and H. D. Betz, Phys. Rev. A **40**, 3632 (1989).

<sup>13</sup>J. E. Borovsky and D. M. Suszcynsky, Phys. Rev. A **43**, 1433 (1991); **43**, 1416 (1991).

<sup>14</sup>H. Rothard, C. Caraby, A. Cassimi, B. Gervais, J. P. Grandin, P. Jardin, M. Jung, A. Billebaud, M. Chevallier, K. O. Groeneveld, and R. Maier, Phys. Rev. A **51**, 3066 (1995).

- <sup>15</sup>A. Billebaud, C. Caraby, A. Cassimi, M. Chevallier, B. Gervais, J. P. Grandin, K. O. Groeneveld, P. Jardin, M. Jung, R. Maier, and H. Rothard, *Nucl. Instrum. Methods Phys. Res. Sect. B* **98**, 492 (1995).
- <sup>16</sup>H. Rothard, A. Billebaud, M. Chevallier, A. Clouvas, B. Gervais, J. P. Grandin, M. Jung, and R. Wünsch, *Nucl. Instrum. Methods Phys. Res. Sect. B* **115**, 284 (1996).
- <sup>17</sup>M. Jung, H. Rothard, B. Gervais, J. P. Grandin, A. Clouvas, and R. Wünsch, *Phys. Rev. A* **54**, 4153 (1996).
- <sup>18</sup>C. R. Vane, S. Datz, P. F. Dittner, H. F. Krause, R. Schuch, H. Gao, and R. Hutton, *Nucl. Instrum. Methods Phys. Res. Sect. B* **79**, 26 (1993).
- <sup>19</sup>H. J. Frischkorn, K. O. Groeneveld, D. Hofmann, P. Koschar, R. Latz, and J. Schader, *Nucl. Instrum. Methods Phys. Res.* **214**, 123 (1983).
- <sup>20</sup>K. Shima, N. Kuno, M. Yamanouchi, and H. Tawara, *At. Data Nucl. Data Tables* **51**, 173 (1992).
- <sup>21</sup>M. J. Gaillard, J. C. Poizat, A. Ratkowski, J. Remillieux, and M. Auzas, *Phys. Rev. A* **16**, 2323 (1977).
- <sup>22</sup>H. Rothard, K. Kroneberger, A. Clouvas, E. Veje, P. Lorenzen, N. Keller, J. Kemmler, W. Meckbach, and K. O. Groeneveld, *Phys. Rev. A* **41**, 2521 (1990).
- <sup>23</sup>A. Clouvas, H. Rothard, M. Burkhard, K. Kroneberger, C. Biedermann, J. Kemmler, K. O. Groeneveld, R. Kirsch, P. Misaelides, and A. Katsanos, *Phys. Rev. B* **39**, 6316 (1989).
- <sup>24</sup>A. Clouvas, A. Katsanos, B. Farizon-Mazuy, A. Farizon, and M. J. Gaillard, *Phys. Rev. B* **43**, 2496 (1991).
- <sup>25</sup>A. Clouvas, A. Katsanos, B. Farizon-Mazuy, M. Farizon, and M. J. Gaillard, and S. Ouaskit, *Phys. Rev. B* **48**, 6832 (1993).
- <sup>26</sup>E. J. Sternglass, *Phys. Rev.* **108**, 1 (1957).
- <sup>27</sup>H. Rothard, J. Schou, and K. O. Groeneveld, *Phys. Rev. A* **45**, 1701 (1992).
- <sup>28</sup>K. Kroneberger, A. Clouvas, G. Schlussler, P. Koschar, J. Kemmler, H. Rothard, C. Biedermann, O. Heil, M. Burkhard, and K. O. Groeneveld, *Nucl. Instrum. Methods Phys. Res. Sect. B* **29**, 621 (1988).
- <sup>29</sup>R. Wünsch (private communication).
- <sup>30</sup>C. Thierfelder, Diplomarbeit IKF, Johann Wolfgang Goethe Universität, Frankfurt, 1996.
- <sup>31</sup>M. Caron (unpublished).
- <sup>32</sup>W. Meckbach, G. Braunstein, and N. Arista, *J. Phys. B* **8**, L344 (1975).
- <sup>33</sup>A. Billebaud, Diplome de Doctorat, IPN Lyon, Lycen-T 9543, 1995.
- <sup>34</sup>H. Rothard, D. Dauvergne, M. Fallavier, K. O. Groeneveld, R. Kirsch, J. C. Poizat, J. Remillieux, and J. P. Thomas, *Radiat. Eff. Defects Solids* **126**, 373 (1993).
- <sup>35</sup>B. Gervais and S. Bouffard, *Nucl. Instrum. Methods Phys. Res. Sect. B* **88**, 355 (1994).
- <sup>36</sup>J. Schou, *Phys. Rev. B* **22**, 2141 (1980).
- <sup>37</sup>P. Sigmund and S. Tougaard, in *Inelastic Particle-Surface Collisions*, Proceedings of the Third International Workshop on Inelastic Ion-Surface Collisions, Feldkirchen-Westerham, Federal Republic of Germany, edited by E. Taglauer and W. Heiland, Springer Series in Chemical Physics Vol. 17 (Springer-Verlag, Berlin, 1981), p. 2.
- <sup>38</sup>J. Devooght, A. Dubus, and J. C. Dehaes, *Phys. Rev. B* **36**, 5093 (1987); **36**, 5110 (1987).
- <sup>39</sup>Software TRIM, J. F. Ziegler and J. P. Biezack, *The Stopping and Ranges of Ions in Solids* (Pergamon, New York, 1985).
- <sup>40</sup>O. Benka, E. Steinbauer, and P. Bauer, *Nucl. Instrum. Methods Phys. Res. Sect. B* **90**, 64 (1994).
- <sup>41</sup>V. P. Zaikov, E. A. Kralkina, V. S. Nikolaev, Y. Fainberg, and N. F. Vorobiev, *Nucl. Instrum. Methods Phys. Res. Sect. B* **17**, 97 (1986).
- <sup>42</sup>O. Benka, A. Schinner, T. Fink, and M. Pfaffenlehner, *Nucl. Instrum. Methods Phys. Res. Sect. B* **115**, 242 (1996).
- <sup>43</sup>P. M. Echenique, R. H. Ritchie, and W. Brandt, *Phys. Rev. B* **20**, 2566 (1979).
- <sup>44</sup>H. Esbensen and P. Sigmund, *Ann. Phys. (N.Y.)* **201**, 152 (1990).